110 (2023) 204901

Contents lists available at ScienceDirect

Gas Science and Engineering

journal homepage: www.journals.elsevier.com/gas-science-and-engineering

Three-dimensional cleat scale modelling of gas transport processes in deformable fractured coal reservoirs

Min Chen *, Shakil A. Masum, Hywel R. Thomas

Geoenvironmental Research Centre, Cardiff School of Engineering, Cardiff University, Queen's Buildings, The Parade, Newport Road, CF24 3AA, Cardiff, UK

ARTICLE INFO

Keywords:
Cleat scale
Adsorption
Hydro-mechanical coupling
DFM modelling
CO_2 geo-sequestration

ABSTRACT

To understand the flow processes in naturally fractured coal reservoirs, a 3D numerical model for coupled gas flow, adsorption and deformation at the scale of coal cleat and matrix blocks is presented in this study. A discrete fracture matrix (DFM) modelling approach has been adopted where flow patterns in fractures and matrices are described separately and explicitly. Different from previous studies in which constant diffusion coefficient, equilibrium adsorption and lumped deformation of matrix and fracture are assumed, in this study, adsorbed gases are treated as an independent phase and the mass exchange process between free phase and adsorbed phase is described using the Langmuir kinetic model. Different gas transport mechanisms in a porous coal matrix are considered for both phase gas transport. Particularly, an equivalent poroelastic continuum model is applied to represent deformation of fracture-matrix system, in which impacts of fracture deformation on the bulk matrix-fracture deformation is accounted for. The hybrid dimensional elements have been employed to discretize the governing equations where fractures are discretized using lower-dimensional interface elements. The accuracy of developed model is validated against experimental results collected from literatures. The simulation results indicate that the gas diffusion process in coal matrices is pressure dependent, surface diffusion of adsorbed gas can contribute to the bulk gas diffusion in coal matrices. Individual cleat initially exhibits a slight opening, followed by significant closure due to adsorption-induced swelling. Ignoring the effect of fracture on bulk deformation, the aperture change is overestimated.

1. Introduction

Coal seams have been broadly recognized as one of the target formations for geological sequestration of carbon dioxide (CO_2) due to their large volume and often collocation with cluster of large, industrial scale, point-source emissions (Masum et al., 2022; Vangkilde-Pedersen et al., 2009). In addition, injection of CO_2 has the potential of enhancing coalbed methane recovery concurrently, which can be used for energy supply and offsetting CO_2 sequestration costs (Cho et al., 2019; Omotilewa et al., 2021). CO_2 sequestration and coalbed methane recovery are complex flow problems and associated with unique structure of coal seams.

Coal is a naturally fractured porous rock composed of fracture network and porous matrix blocks, as shown in Fig. 1(a). When gas is injected in coalbeds, it firstly flows through fractures, and then diffuses into porous coal matrices. Coal matrix contains numerous pores, which provide the potential sites that have strong affinity to certain gases, such as CO_2, CH_4 (Chen et al., 2022; Shi and Durucan, 2003), as shown in Fig. 1(b). Fracture network provides the main flow channel for fluid flow, which is generally controlled by the fracture aperture. However, majority of the studies represent permeation of coalbeds in terms of coal permeability rather than direct measurement of change in fracture aperture (Pan and Connell, 2012). Recently, Chen et al. (2020a) presented a two dimensional discrete fracture model of coupled fluid flow, adsorption and geomechanics to study dynamic behaviors of fractures in coal. From the numerical modelling study, they reported that fracture aperture reduced significantly due to adsorption induced coal-swelling. Bertrand et al. (2019) reported that prediction based on porosity evolution can largely deviate from the direct fracture aperture models, and numerical models at the scale of the matrix and the cleats should be considered.

Gas transport in a coal matrix is the intermediate or rate-controlling step of gas migration (Chen et al., 2020b), and critical for successful, long term CO_2 storage and CH_4 production. Gas migration in porous coal matrix consists of two important processes: gas diffusion and adsorption/desorption. The widely used approach to obtain diffusivity of gas in coal matrices is conversion of kinetic data into diffusion rates using

---

* Corresponding author.
E-mail address: chenm24@cardiff.ac.uk (M. Chen).

https://doi.org/10.1016/j.jgsce.2023.204901
Received 15 November 2022; Received in revised form 18 December 2022; Accepted 18 January 2023

Nomenclature

a	Spacing between fractures
$\mathbf{B}$	Strain displacement matrix
b_{eff}	Biot's effective stress coefficient
b_s	Slip coefficient
C_f	Gas concentration in fractures
C_L	Maximum adsorbed phase concentration
C_m	Gas concentration in coal matrices
C_s	Adsorbed phase concentration
$\boldsymbol{C}_{f'}$	Compliance matrices for fracture
$\boldsymbol{C}_{m'}$	Compliance matrices for matrix
d_f	Fractal dimension of the pore surface
d_m	Normalized molecular size
D_K	Knudsen diffusivity
D_s	Surface diffusion coefficient
D_s^0	Surface diffusivity at zero coverage
D_v	Viscous flow-induced diffusivity
E	Young's modulus of coal matrix
G	Shear modulus
K_n	Knudsen number
K_{ns}	Normal fracture stiffness
K_{ns0}	Initial normal fracture stiffness
K_{sh}	Normal and shear fracture stiffness
k_∞	Intrinsic permeability of porous media
M	Molar weight
N_I	Shape function
n	Porosity of coal matrix
p_f	Gas pressure in fractures
p_L	Pressure constant of Langmuir isotherm
p_m	Gas pressure in coal matrices
r_h	Hydraulic radius of the pore
R	Universal gas constant
S	Sink/source term
T	Temperature
$\mathbf{u}$	Displacement
$\mathbf{v}_f$	Flow velocity
Z_f	Gas compressibility factor
Γ_{fm}	Fracture-matrix mass transfer term
μ	Gas viscosity
ω_K	Weighting coefficient for Knudsen flow
ω_v	Weighting coefficient for viscous flow
τ	Tortuosity of the porous medium
θ	Gas coverage on the micropore wall
γ_a	Rate constants for adsorption
γ_d	Rate constants for desorption
v	Poisson's ratio
$\boldsymbol{\sigma}$	Total stress tensor
$\boldsymbol{\sigma}^e$	Effective stress tensor
σ_n'	Effective normal stress acting at fracture surface
$\boldsymbol{\varepsilon}$	Strain vector
ε_L	Volumetric strain coefficient of gas
$\boldsymbol{\varepsilon}^e$	elastic strain vector
$\boldsymbol{\varepsilon}^s$	Sorption-induced strain
w	Hydraulic aperture of fractures
w_m	Maximum closure of the fracture aperture
Δw	Change in fracture aperture
W	Ratio of rate of blockage to forward migration

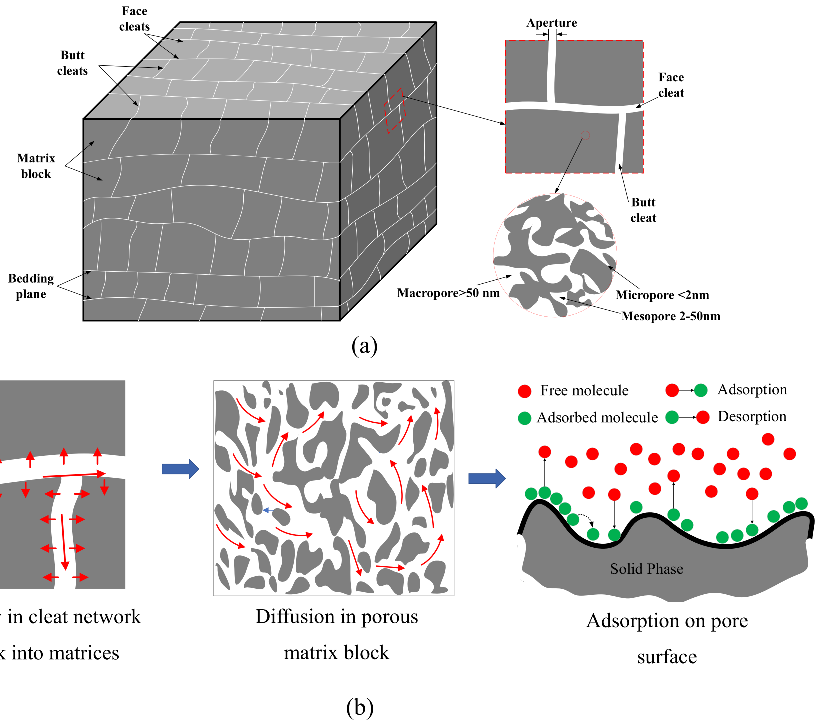

Fig. 1. (a) 3D schematic of naturally fractured coal and (b) representation of gas transport process in fractured coal.

elapsed time during the adsorption/desorption processes (e.g. Busch et al., 2004; Pillalamarry et al., 2011; Sadasivam et al., 2022). Zhao et al. (2019) presented a detailed review on the models of gas diffusion in coals including analytical and empirical models. The unipore diffusion (UD) model and bidisperse diffusion (BD) model are two widely used diffusion models to study diffusion behavior in coal matrix. Some studies

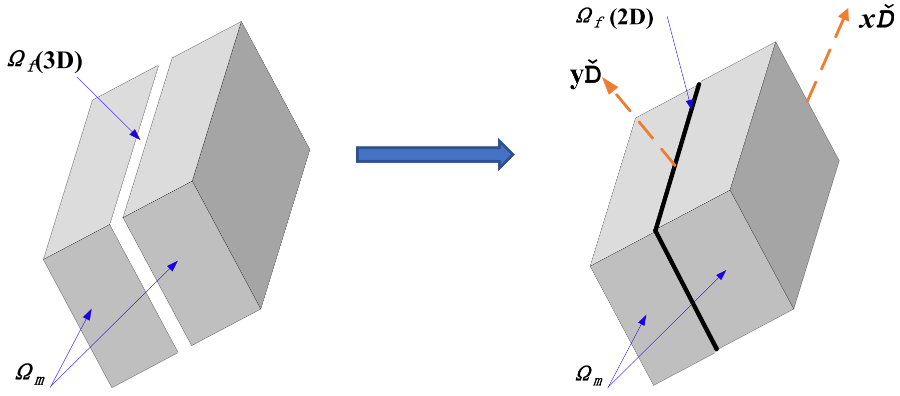

Fig. 2. Schematic representation of the discrete fracture matrix approach (x'-y' is local coordinate).

suggested that the UD model with only one characteristic diffusion coefficient is sufficient to describe the adsorption kinetics of gases in coals (e.g. Charrière et al., 2010; Pone et al., 2009). The study by Clarkson and Bustin (1999) compared the UD and BD models for dull and bright coals of different pore sizes, it was reported that the UD model was able to capture sorption kinetics of gases in some bright coals, however, UD model was insufficient to describe dynamic adsorption-diffusion processes of gases in most coals with multimodal pore distributions. In contrast, BD model, which has two characteristic diffusion coefficients, shows the capacity of capturing the sorption kinetics in multimodal coals (Busch et al., 2004; Clarkson and Bustin, 1999; Cui et al., 2004). On the other hand, in these models, the diffusion coefficients are assumed to be constant, which contradicts experimental observations. For example, Charrière et al. (2010) observed that the adsorption kinetics of CO_2 and CH_4 in coal is pressure- and temperature-dependent. Furthermore, application of these models to field studies is not realistic or feasible due to complex mathematical procedures and difficulties in obtaining the model parameters for coals. Therefore, more attempts are required to address these issues on sorption kinetics involved in gas migration in coals.

The purpose of this study is to develop a three-dimensional cleat scale model for coupled compressible gas flow and geomechanics in a deformable fractured coal. The free phase and adsorbed phase gas are treated separately based on relevant gas transport mechanisms. The mass exchange between these phases is described by a Langmuir kinetics. Instead of traditional dual porosity model which assumes fracture network as a continuum, the fracture flow in present model is represented explicitly through discrete fracture matrix model. An equivalent poroelastic continuum model is applied to account for the effect of facture deformation on the bulk fracture-matrix deformation. In the subsequent sections, firstly, the governing equations for gas phases transport and deformation are presented, followed by numerical solutions in section 3. Section 4 presents the validation tests of the proposed model against experimental results to confirm reliability of the developed model. Finally, in Section 5, an application of the model to investigate the coupled transport and deformation processes of gases in coal at the cleat scale is detailed. The conclusions are drew in section 6.

2. Model development

In this work, the discrete fracture matrix (DFM) model is employed to represent flow processes in discrete fractures and porous rock matrices. Discrete fracture is idealized as a lower-dimensional geometric object. For example, a 2D plane represents fractures in 3D problems, as shown in Fig. 2. The whole domain Ω is:

$$\Omega = \Omega_m \cup \sum_d w_m \times \Omega_{f,d} \tag{1}$$

in which Ω_m represents the domain occupied by matrix, $\Omega_{f,d}$ is the domain occupied by the dth discrete fracture, and w_m is the mechanical aperture of fracture.

Below, a set of filed equations for gas transport and coal deformation are developed based on the following assumption: 1) Coal is considered to be a dry; 2) Coal matrix is homogeneous, isotropic and elastic; 3) The strain is small; 4) The coal is isothermal; 5) Gas exists as free phase in natural fractures, however, it may be free or adsorbed phase in the coal matrix. Both phases obey the principle of mass conversation; In the following, the subscript *m* denotes the matrix and the subscript *f* denotes the fractures.

2.1. Gas transport

2.1.1. Free gas flow in fractures

The governing equation for gas flow in fractures is expressed as:

$$\frac{\partial}{\partial t}\left(C_f w_h\right) = -w_h \nabla_l \bullet \left(\mathbf{v}_f C_f\right) - \Gamma_{fm} \tag{2}$$

where C_f is the gas concentration in fractures, w_h is hydraulic aperture of fractures, $\mathbf{v}_f$ is the flow velocity along the longitudinal direction of fracture and Γ_{fm} is the fracture-matrix mass transfer term. ∇_l is the lower dimensional gradient operator, for 3D problems, ∇_l can be expressed as $\nabla_l = \frac{\partial}{\partial x'} + \frac{\partial}{\partial y'}$ $x' - y'$ is local coordinate, x' axis and y' axis are parallel to fracture surface, as shown in Fig. 2, they are generally not consistent with the global coordinate.

The longitudinal flow velocity $\mathbf{v}_f$ is described as (van Golf-Racht, 1982):

$$\mathbf{v}_f = -\frac{w^2}{12\mu}\nabla_l p_f \tag{3}$$

$$p_f = Z_f RTC_f \tag{4}$$

where μ is the gas viscosity, p_f is the gas pressure in fractures, Z_f is the gas compressibility factor, R is the universal gas constant and T is temperature. In this work, the Equations of State proposed by Peng and Robinson (1976) is used to calculate the compressibility factor and the gas viscosity is described by Chung et al.'s approach (Poling et al., 2001).

2.1.2. Free gas diffusion in coal matrices

Based on the principle of mass conservation, the mass balance equation for a free gas in porous matrices can be expressed as (Chen et al., 2020b, 2021; Cui et al., 2022):

$$\frac{\partial(n_e C_m)}{\partial t} = \nabla \bullet (\omega_K D_K + \omega_v D_v)\nabla C_m + \Gamma_{fm} - S \tag{5}$$

where $n_e = n\left(\frac{r_e}{r_h}\right)^2$, n is the porosity of coal matrix in absence of gas adsorption, $r_e = r_h - d_m\theta$, r_h is the hydraulic radius of the pore, d_m is the normalized molecular size, θ is the gas coverage on the micropore wall. The term in bracket on right hand side is the total gas flux in the free phase, $\omega_K = \frac{K_n}{1+K_n}$ and $\omega_v = \frac{1}{1+K_n}$ are two weighting factors for measuring the contributions from Knudsen diffusion and viscous flow to free gas migration, respectively (Chen et al., 2020b; Wu et al., 2016). K_n is Knudsen number, D_K is Knudsen diffusivity and D_v is viscous flow-induced diffusivity, S is the sink/source term allowing for mass exchange between free phase and adsorbed phase, which will be detailed later.

Knudsen number (K_n) is defined as the ratio of a molecular mean free path to the average pore diameter (Javadpour et al., 2007; Villazon et al., 2011):

$$K_n = \frac{\mu}{2r_e p_m}\sqrt{\frac{\pi ZRT}{2M}} \tag{6}$$

where $p_m = Z_m RTC_m$ is the gas pressure in matrices and M is the molar weight.

Following Darabi et al. (2012), the Knudsen diffusion coefficient D_K is given as:

$$D_K = \frac{2r_e}{3}\frac{n_e}{\tau}\left(\frac{d_m}{2r_e}\right)^{d_f-2}\sqrt{\frac{8ZRT}{\pi M}} \tag{7}$$

where τ is tortuosity of the porous medium, d_f is the fractal dimension of the pore surface accounting for the effect of pore-surface roughness.

Following the work by Chen et al. (2021), the viscous flow-induced diffusivity D_v can be expressed as:

$$D_v = \left(\frac{r_e}{r_h}\right)^4 \frac{k_\infty}{\mu} u(1+\alpha_r K_n)\left(1+\frac{4K_n}{1-b_s K_n}\right)\left(1+\frac{C_m}{Z}\frac{\partial Z}{\partial C_m}\right) \tag{8}$$

where $k_\infty = \frac{n}{\tau}\frac{r_h^2}{8}$ represents the intrinsic permeability of porous media, $\alpha_r = 1.358\left(1+\frac{0.178}{K_n^{0.4348}}\right)^{-1}$ is the rarefaction coefficient, b_s is the slip coefficient (here $b_s = -1$) associated with slippage effect (Civan, 2010).

2.1.3. Adsorbed gas transport

Surface diffusion is considered to be the dominant mode of transport for adsorbed gases, and the adsorbed gas concentration gradient is the driven force for surface diffusion (Wu et al., 2016; Xiong et al., 2012). Considering the principle of mass conversation, the governing transport equation for adsorbed gas can be expressed as (Chen et al., 2020b):

$$\frac{\partial[(1-n)C_s]}{\partial t} = \nabla \bullet (1-n)D_s\nabla C_s + S \tag{9}$$

where C_s is the adsorbed phase concentration and D_s is the surface diffusion coefficient.

Under isotherm conditions, surface diffusivity depends on the adsorbed gas concentration, the following relationship propose by Chen and Yang (1991) is adopted here:

$$D_s = D_s^0\frac{1-\theta+\frac{W}{2}\theta(1-\theta)+(1-W)\frac{W}{2}\theta^2 H(1-W)}{\left(1-\theta+\frac{W}{2}\theta\right)^2} \tag{10}$$

$$H(1-W) = \begin{cases} 0 & W \geq 1 \\ 1 & 0 \leq W < 1 \end{cases} \tag{11}$$

where D_s^0 is the surface diffusivity at zero coverage, W is defined as the ratio of the rate of blockage to the rate of forward migration, which is a measure of the degree of blockage by another adsorbed molecule (Chen and Yang, 1991).

It is believed that the gas adsorption obeys the Langmuir adsorption isotherm and, therefore, the gas coverage θ can be described as:

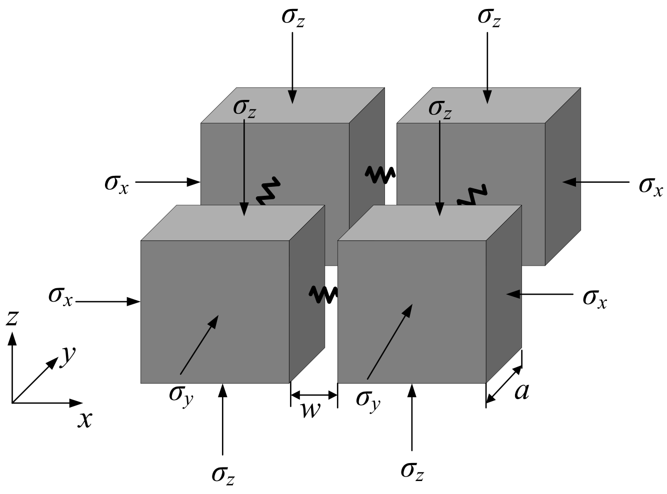

Fig. 3. Schematic of fracture-matrix system with 3D loading.

$$\theta = \frac{C_s}{C_L} \tag{12}$$

where C_L is the maximum adsorbed phase concentration.

2.1.4. Mass exchange between free gas and adsorbed gas phases

Mass interchange between adsorbed and free phase can be characterized by the adsorption kinetics, as shown in Fig. 1(b). Considering Langmuir kinetics, the gas adsorption rate, R_a, and desorption rate, R_d, can be expressed as (Do and Wang, 1998):

$$R_a = \gamma_a p_m(C_L - C_s) \tag{13}$$

$$R_d = \gamma_d C_s \tag{14}$$

where γ_a and γ_d are the rate constants for adsorption and desorption, respectively.

Therefore, the net rate of adsorption, R_{net}, can be given as:

$$R_{net} = R_a - R_d = \gamma_d[B_L p_m(C_L - C_s) - C_s] \tag{15}$$

where $\gamma_a/\gamma_d = B_L = 1/p_L$, p_L is pressure constant of Langmuir model.

The mass exchange term between free and adsorbed phases in equations (5) and (9) can be given as:

$$S = (1-n)\gamma_d[B_L p_m(C_L - C_s) - C_s] \tag{16}$$

2.2. Deformation of fractured porous rock

Matrix blocks are generally surrounded by cleats, however, they are in reality not completely separated from each other by fractures, but connected by the matrix “bridges” (Liu and Rutqvist, 2010). The mechanical behavior of the fractured rock can be divided into two processes: when the dual system is compressed, the fracture firstly undergoes deformation because of its lower stiffness. Normal and shear fracture stiffness are usually introduced to qualify the fracture deformation. While the fractures are nearly closing, the stiffness of the rock tends to be identical to that of the intact rock matrix, the fracture and matrix will deform together (Bertrand et al., 2017). Therefore, lump deformation of both matrix and fracture together should be considered.

Matrix bridges connect the adjacent matrix blocks like springs (e.g. Gu and Chalaturnyk, 2006), as shown in Fig. 3. Considering the fracture-matrix system at 3D stress state shown in Fig. 3, the relationship between changes in total stress and the effective stress can be written in incremental form as:

$$d\boldsymbol{\sigma} = d\boldsymbol{\sigma}^e - b_{eff}\mathbf{m}dp \tag{17}$$

where $\boldsymbol{\sigma}$ is total stress tensor, the current formulation considers a positive sign convention for tensile stress. $\boldsymbol{\sigma}^e$ is effective stress tensor, $\mathbf{m}$ is a vector, $\mathbf{m}^T = (1, 1, 1, 0, 0, 0)$ for three dimensions, b_{eff} is the Biot's effective stress coefficient.

Deformation of coal is composed of mechanical deformation due to effective stress and adsorption-induced swelling, and it can be described as:

$$d\boldsymbol{\varepsilon} = d\boldsymbol{\varepsilon}^e + d\boldsymbol{\varepsilon}^s \tag{18}$$

where $\boldsymbol{\varepsilon}$ is the total strain vector, $\boldsymbol{\varepsilon}^e$ is the elastic strain vector, $\boldsymbol{\varepsilon}^s$ is the sorption-induced swelling strain. A linear relationship between swelling strain and total adsorbed amount of gas is usually employed to calculate swelling strain (e.g. Cui et al., 2007):

$$d\varepsilon^s = \frac{1}{3}\varepsilon_L dC_s \tag{19}$$

where ε_L is the volumetric strain coefficient of gas.

The total elastic strain increment due to deformation of matrix and fracture is expressed as:

$$d\boldsymbol{\varepsilon}^e = d\boldsymbol{\varepsilon}^e_f + d\boldsymbol{\varepsilon}^e_m \tag{20}$$

The elastic strain for individual region is:

$$d\boldsymbol{\varepsilon}^e_m = \boldsymbol{C}_{m'}\, d\boldsymbol{\sigma}^e \tag{21}$$

$$d\boldsymbol{\varepsilon}^e_f = \boldsymbol{C}_{f'}\, d\boldsymbol{\sigma}^e \tag{22}$$

where $\boldsymbol{C}_{m'}$ and $\boldsymbol{C}_{f'}$ are the compliance matrices for matrix and fracture region, respectively, given as:

$$\boldsymbol{C}_{m'} = \begin{bmatrix} \frac{1}{E} & -\frac{v}{E} & -\frac{v}{E} & 0 & 0 & 0 \\ -\frac{v}{E} & \frac{1}{E} & -\frac{v}{E} & 0 & 0 & 0 \\ -\frac{v}{E} & -\frac{v}{E} & \frac{1}{E} & 0 & 0 & 0 \\ 0 & 0 & 0 & \frac{1}{2G} & 0 & 0 \\ 0 & 0 & 0 & 0 & \frac{1}{2G} & 0 \\ 0 & 0 & 0 & 0 & 0 & \frac{1}{2G} \end{bmatrix}$$

$$\boldsymbol{C}_{f'} = \begin{bmatrix} \frac{1}{K_n a} & 0 & 0 & 0 & 0 & 0 \\ 0 & \frac{1}{K_n a} & 0 & 0 & 0 & 0 \\ 0 & 0 & \frac{1}{K_n a} & 0 & 0 & 0 \\ 0 & 0 & 0 & \frac{1}{K_{sh} a} & 0 & 0 \\ 0 & 0 & 0 & 0 & \frac{1}{K_{sh} a} & 0 \\ 0 & 0 & 0 & 0 & 0 & \frac{1}{K_{sh} a} \end{bmatrix}$$

where E is the Young's modulus of coal matrix, v is Poisson's ratio, and G is the shear modulus, K_{ns} and K_{sh} are normal and shear fracture stiffness, a is the spacing between fractures.

The normal stiffness of fracture is generally not constant but sensitive to normal fracture aperture. The change in normal stiffness for a fracture can be evaluated using the empirical model proposed by Bandis et al. (1983):

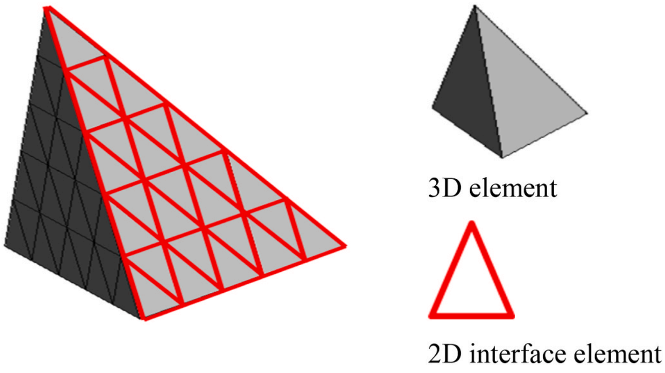

Fig. 4. Schematics of conforming mesh: porous matrix is discretized with the 3D elements and fracture is discretized with 2D triangular elements.

$$K_{ns} = \frac{K_{ns0}}{1 - \frac{\Delta w}{w_m}} \tag{23}$$

Where K_{ns0} is the initial normal fracture stiffness, w_{mm} is the maximum closure of the fracture aperture and $\Delta w = \frac{\sigma_n' w_{mm}}{\sigma_n' + K_{n0} w_{mm}}$ is the change of fracture aperture, σ_n' is effective normal stress acting at the fracture surface (Chen et al., 2020a), w_m is mechanical aperture of fractures, which is different from hydraulic aperture and can be determined by direct measurements. Because of the influences of surface roughness, tortuosity etc. The mechanical aperture is generally larger than the corresponding hydraulic apertures (Gu and Chalaturnyk, 2010). The empirical model presented by Barton et al. (1985) can be used to describe the relationship between hydraulic apertures and mechanical apertures:

$$w_h = \begin{cases} \dfrac{{w_m}^2}{JCR^{2.5}} & JCR > 0 \\ w_m & \text{otherwise} \end{cases} \tag{24}$$

where JCR is the joint roughness coefficient with zero value representing smooth plane surfaces, in such case the hydraulic aperture is the mechanical one, it is noteworthy that the unit of apertures is micron here. Bastola and Chugh (2015) tested the roughness coefficient for coal, which ranges from 2 to 12.

The strain is related to displacement, expressed as:

$$d\boldsymbol{\varepsilon} = \mathbf{B}d\mathbf{u} \tag{25}$$

where $d\mathbf{u}$ is a vector of the incremental displacement, $\mathbf{B}$ is the strain displacement matrix.

The stress equilibrium equation with ignoring body force is given as:

$$\mathbf{B}^T d\boldsymbol{\sigma} = 0 \tag{26}$$

Substituting Eq. (17)–(22) into Eq. (26) produces:

$$\mathbf{B}^T \boldsymbol{D}_{mf}\mathbf{B}d\mathbf{u} - \mathbf{B}^T\mathbf{m}b_{eff}dp - \varepsilon_L \mathbf{B}^T\boldsymbol{D}_{mf}\mathbf{m}dC_s = 0 \tag{27}$$

where $\boldsymbol{D}_{mf} = (\boldsymbol{C}_f + \boldsymbol{C}_m)^{-1}$.

3. Numerical solutions

In this work, the finite element method is used to obtain the numerical solutions. The unknown variables, C_m, C_f, C_s and $\mathbf{u}$ are selected as the primary variables. Hybrid dimensional elements are used to spatially discretize the computational domain. The lower-dimensional interface elements, $\boldsymbol{N}_{If}$, are employed to discretize the fractures, while matrix domains are discretized with higher-dimensional elements, $\boldsymbol{N}_{Im}$. Fig. 4 shows the generated conforming mesh where interface elements

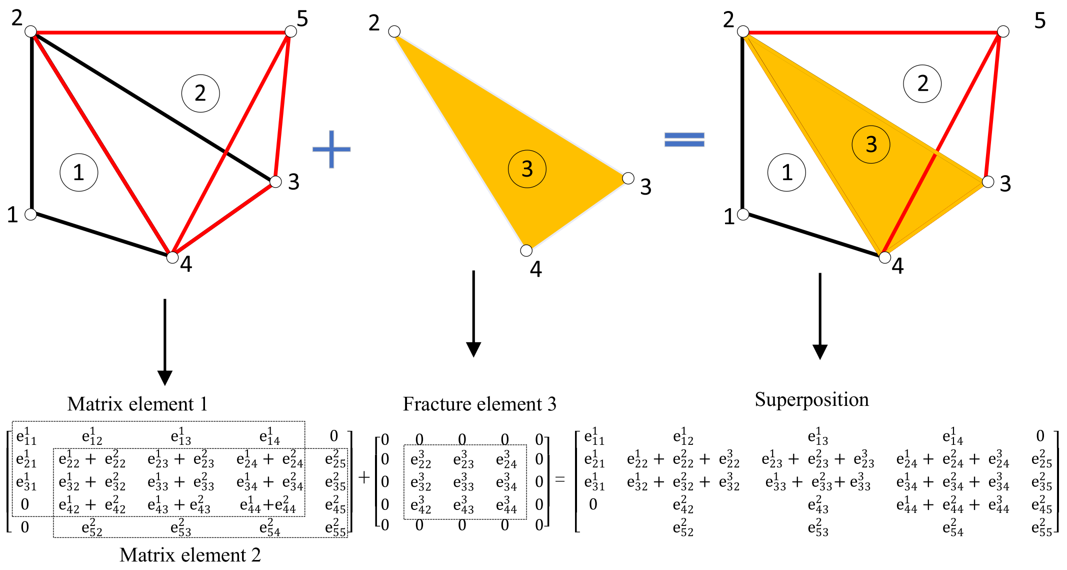

Fig. 5. Assembly process of the matrix and fracture flow equations into the stiffness matrix.

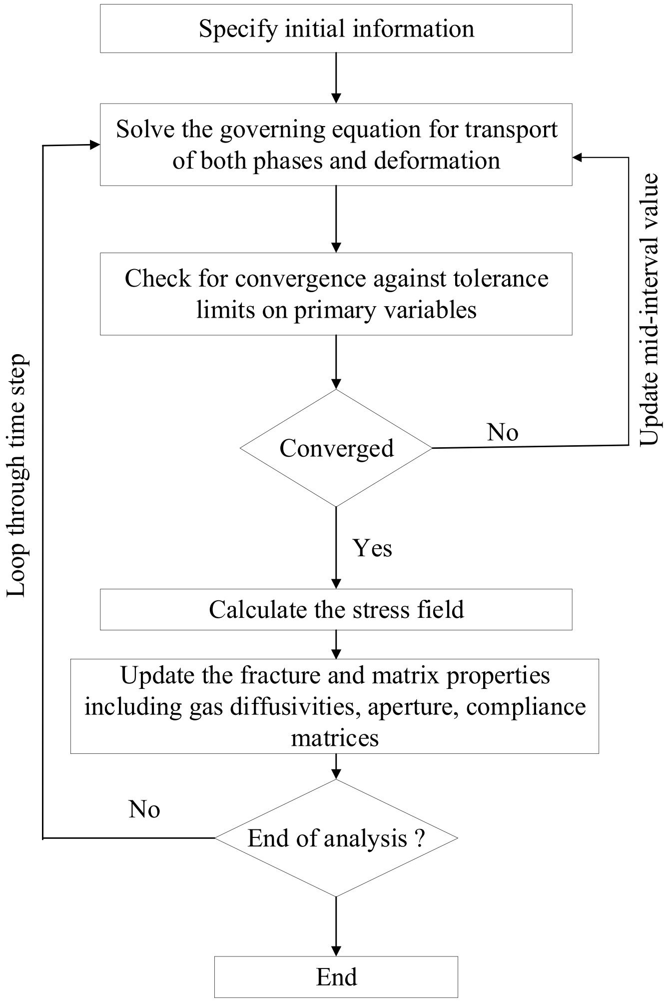

Fig. 6. Implementation procedure for developed numerical model in computer code.

for fractures are located on the edges of grids for matrix domain, two types of elements share the same nodes. By means of shape functions, the primary variables are approximated by interpolating the variables at nodes, written as:

$$\widehat{C}_m(\mathbf{x},\mathrm{t}) = \sum_{I_m\in\mathcal{N}_m} N_{I_m}(\mathbf{x})C_{I_m}(t) \tag{28a}$$

$$\widehat{C}_f(\mathbf{x},\mathrm{t}) = \sum_{I_f\in\mathcal{N}_f} N_{I_f}(\mathbf{x})C_{I_f}(t) \tag{28b}$$

$$\widehat{C}_s(\mathbf{x},\mathrm{t}) = \sum_{I_m\in\mathcal{N}_m} N_{I_m}(\mathbf{x})C_{I_s}(t) \tag{28c}$$

$$\widehat{\mathbf{u}}(\mathbf{x},\mathrm{t}) = \sum_{I_m\in\mathcal{N}_m} N_{I_m}(\mathbf{x})\mathbf{u}_{I_m}(t) \tag{28d}$$

where N_{I_m} and N_{I_f} are shape functions of node I_m and I_f for the discretized porous domain and fracture domain, respectively. $\mathcal{N}_m$ and $\mathcal{N}_f$ are the number of nodes in the elements for discretization of porous matrix domain and fracture domain, respectively.

Due to the fact that width of fracture is orders of magnitude lower than its length, it c assumed that the flow variables are continuous over the fracture width i.e. $C_m = C_f$ so that the calculation of mass exchange term between the free gas transport in fracture and matrix is not required with the principle of superposition (Chen et al., 2020a). The assembly process of the discretized transport equations for free gas in fractures and matrices into the stiffness matrix is shown in Fig. 5. It is worth mentioning that the local coordinate system for discrete fracture is generally not consistent with global coordinate system. For numerical implementation, the local coordinate system should be transformed into the global coordinate system. This numerical algorithm has been implemented into the in-house finite element-based computer code, which is incrementally developed at Cardiff University (e.g. Chen et al., 2020a; Hosking et al., 2020; Thomas and He, 1995; Thomas et al., 1998).

The numerical implementation procedures for the developed coupled gas flow, adsorption and deformation model is illustrated in Fig. 6. A sequential implicit numerical scheme is adopted here. After the initial information including material properties, boundary conditions and initial conditions, the solutions of governing equations for both phase gas transport and coal deformation (Eqs. ((2), (5), (9) and (26)) can be obtained by iteration until convergence is achieved. And then, the

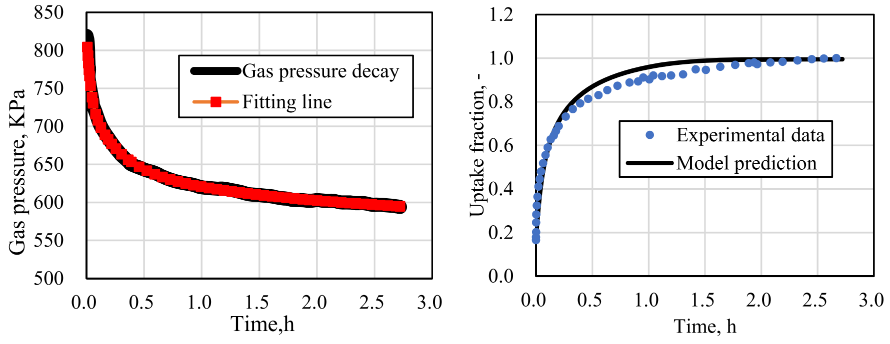

(a) (b)

Fig. 7. (a) The boundary gas pressure applied at the external surface of the sample for the validation test, which is obtained by fitting the pressure decay results and (b) Comparison between model predicted results and experimental tests of Wang et al. (2017).

Table 1
Parameters used in the proposed model for validation test.

Parameters	Values
Temperature, T (K)	303
Gas molar mass, M (kg/mol)	0.028
Universal gas constant, R (J/mol/K)	8.314
Pressure constant of Langmuir model, p_L (MPa)	4.44
Volume constant of Langmuir model, C_L (mol/m^3)	1062
Molecular diameter of gas, d_m (nm)	0.36
Pore radius, r_h (nm)	1.1
Fractal dimension of the pore surface, d_f (−)	2.0
Surface diffusion, D_s^0 (m^2/s)	1.2e-12
Ratio of rate constant, w (−)	0.0
Rate constant of desorption, γ_d (s^{-1})	2.8e-4
Porosity-tortuosity factor, $n/\ \tau$ (−)	1.11e-5
Porosity, n (−)	0.049
Solid density, ρ (kg/m^3)	1440

material properties like gas diffusivities, fracture aperture are updated in each timestep based on the results obtained the previous time step. The numerical implementation will end until the specified simulation time is reached.

4. Model validation

In this section, two important subsets of the numerical model were validated here: i) the adsorption kinetics, and ii) the noninear mechanical behavior of coal. The model predicted results are compared with relevant experimental data collected from literatures. More validation exercises can be found in our previous work, including the role of discrete fractures in flow process and numerical algorithm (Chen et al., 2020a, 2022).

4.1. Adsorprion kinetics

Wang et al. (2017) conducted experimental test on a nitrogen (N_2) diffusion (adsorption kinetic) in coals. A modified manometric method was adopted in his work. Bulk coal sample from Bulli coal seam, Sydney Basin of Australia was collected, crushed and sieved to 2.36–3.35 mm particles. The experimental temperature of their study was 303 K. The details of experimental procedures are available in Wang et al. (2017). The experimental data on gas uptake fraction (defined as the ratio of adsorbed amount at any time to final adsorbed amount at a certain pressure condition) is used as benchmark for this validation exercise.

The coal particle is assumed to be a sphere with radius of 1.43 mm for numerical simulation and the N_2 adsorption behavior in coal matrix follows Langmuir isotherm. The measured pressure decay curve (Fig. 6 (a)) of Wang et al. (2017) is used as the boundary condition assigned on the external surface of the domain for free phase gas. An exponential decay fitting function is selected to represent the pressure decay curve, as shown in Fig. 7(a). The initial gas pressure is set to the atmospheric pressure of 0.1 MPa This value is estimated according to the initial uptake fraction and gas pressure at equilibrium state. Fig. 7(a) shows that the gas pressure drops to about 0.6 MPa when equilibrium state is reached. According to the Langmuir isotherm, the amount of adsorbed gas is about 3.54 kg/m^3. Since the initial amount of adsorbed gas accounts for 18% of amount of adsorbed at equilibrium state, i.e. 0.637 kg/m^3. With the help of Langmuir isotherm, the initial pressure is estimated to be about 0.1 MPa. The gas pressure boundary and initial gas pressure were converted to the equivalent free gas concentrations using the real gas law in simulation. Table 1 lists the material parameters used for this validation test, some of which are chosen from Wang et al. (2017), others are obtained by fitting the experimental results. The total adsorbed amount of gas is obtained via the sum of volume integrations for spherical domain. Fig. 7(b) shows that the model results compare well with the experimental result, indicating that the developed model describe the transport processes of adsorptive gas in coal matrix sufficiently and adequately.

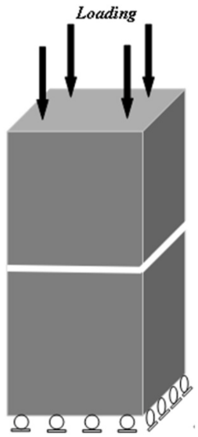

Fig. 8. Geometry and boundary conditions for validation test.

4.2. Uniaxial compression test

This subsection examines validity of the proposed model to describe mechanical behavior of coal. This has been achieved by comparing the model predicted results against the observed experimental data of Czaplinski and Gustkiewicz (1990). Gu and Chalaturnyk (2006) introduced experimental tests carried out by Czaplinski and Gustkiewicz (1990). The experimental data on a uniaxial compression test is set as benchmark for evaluating the applicability of the proposed model. In the

Table 2
Parameters used for matching experimental data.

Parameters	Value
Young's modulus, E, (GPa)	1.8
Poisson ratio, v, (-)	0.18
Fracture spacing, a, (cm)	2.4
Initial normal stiffness, K_{n0}, (GPa/m)	28.8
shear stiffness, K_{sh}, (GPa/m)	3.6
Maximum closure, w_m, (mm)	0.1
Initial aperture, w, (mm)	0.11

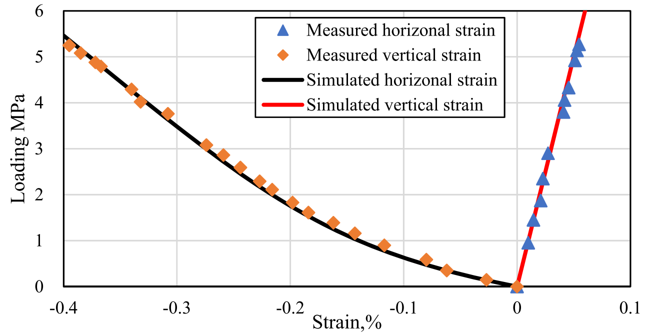

Fig. 9. Comparison between experimental data and model prediction of uniaxial compression.

numerical simulation, a prism is applied to represent the fractured coal, as shown in Fig. 8. A vertical constraint is applied to the bottom boundary while a loading stress is applied to top surface of the prism. No constrain is assigned to the lateral sides. Both matrix and fracture are assumed to be isotropic. The material properties used in this simulation is chosen from Gu and Chalaturnyk (2006) except for the cleat aperture, which is estimated via matching the test results, as listed in Table 2. The estimated cleat aperture is 0.11 mm, higher than the estimated values presented by Gu and Chalaturnyk (2006), but falls within the range of 0.002–2.02 mm measured by Weniger et al. (2016). The comparison between model prediction and laboratory test is shown in Fig. 9.

It can be seen from Fig. 9 that the horizonal strain exhibits an obviously linear correlation with stress, while linear vertical strain evolution with stress only occurs as a result of the compression of the coal matrix when the stress is higher. There is a concave part for curves of strain versus stress in vertical direction under lower stresses, this is due to the fact that initial normal stiffness of fracture is lower because of larger fracture opening, stress can lead to a relatively larger strain (Gu and Chalaturnyk, 2006). With fracture closure, the stiffness tends to that of intact sample, the fracture and matrix starts to deform simultaneously. The model results compare well with the experimental measurement, indicating that the model can describe deformation of fractured porous rocks accurately.

5. Model application

5.1. Simulation setup

A typical coal structure consists of two distinct sets of natural fractures. The dominant fracture system is more continuous face cleat. The secondary fracture system known as butt cleat is usually perpendicular to the face cleat and is less continuous (Laubach et al., 1998; Seidle, 2011). Based on the characteristics of cleat distribution, a simplified coal cleat network is designed, as shown in Fig. 10 (a). The generated 3D geometrical model of 4 cm × 3 cm × 0.5 cm is used for simulation domain, including 3 face cleats (blue lines) and 18 butt cleats (yellow lines) with spacing of 1 cm. The model domain is discretized with unstructured tetrahedral elements, as shown in Fig. 10(b). A finer grid is designed to capture the area around the cleats.

Two measuring points, P1 (0.6 cm, 0.6 cm, 0.25 cm) closed to cleat and P2 (1 cm, 1.0 cm, 0.25 cm) in centre of matrix block are set to monitor the variations of the gas pressures and adsorbed concentration and P3 (1.5 cm, 1.0 cm, 0.25 cm) is used to monitor the evolution of cleat aperture. CO_2 is selected as the injection gas. To explore the effect of pressure on gas transport behavior in coal matrix, three different gas pressures, e.g., 2, 4 or 6 MPa are prescribed individually at left corner of the domain. Horizontal displacement constrain is applied to lateral sides

Table 3
Parameters used for numerical simulation.

Parameters	Values
Reference temperature, T_0 (K)	308
Density of coal, ρ_s (kg/m^3)	1250
Initial porosity, n (−)	0.05
Porosity-tortuosity factor, n/τ (−)	1.15e-5
Gas molar mass, M (kg/mol)	0.044
Langmuir pressure constant, p_L (MPa)	1.13
Langmuir volume constant, C_L (mol/kg)	1.56
Pore radius, r_h (nm)	2.0
Surface diffusion, D_s^0 (m^2/s)	2.0e-12
Rate constant for desorption, γ_d (s^{-1})	5.0e-5
Fractal dimension of the pore surface, d_f (−)	2.0
Young's modulus, E, (GPa)	3.0
Poisson's ratio, v, (−)	0.3
Initial normal stiffness, K_{n0}, (GPa/m)	5
Shear stiffness, K_t, (GPa/m)	50
No-load fracture aperture, w_0 (mm)	0.5
Maximum fracture aperture closure, w_m, (mm)	0.49
Roughness coefficient, JCR,-	2.0
Volumetric strain coefficient, ε_L, (m^3/mol)	1.8e-5

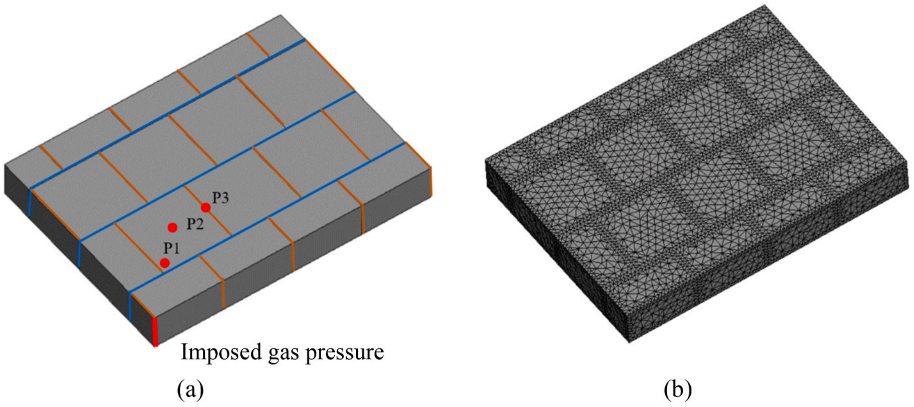

Fig. 10. (a) Geometric model and (b) Unstructured mesh for numerical simulation.

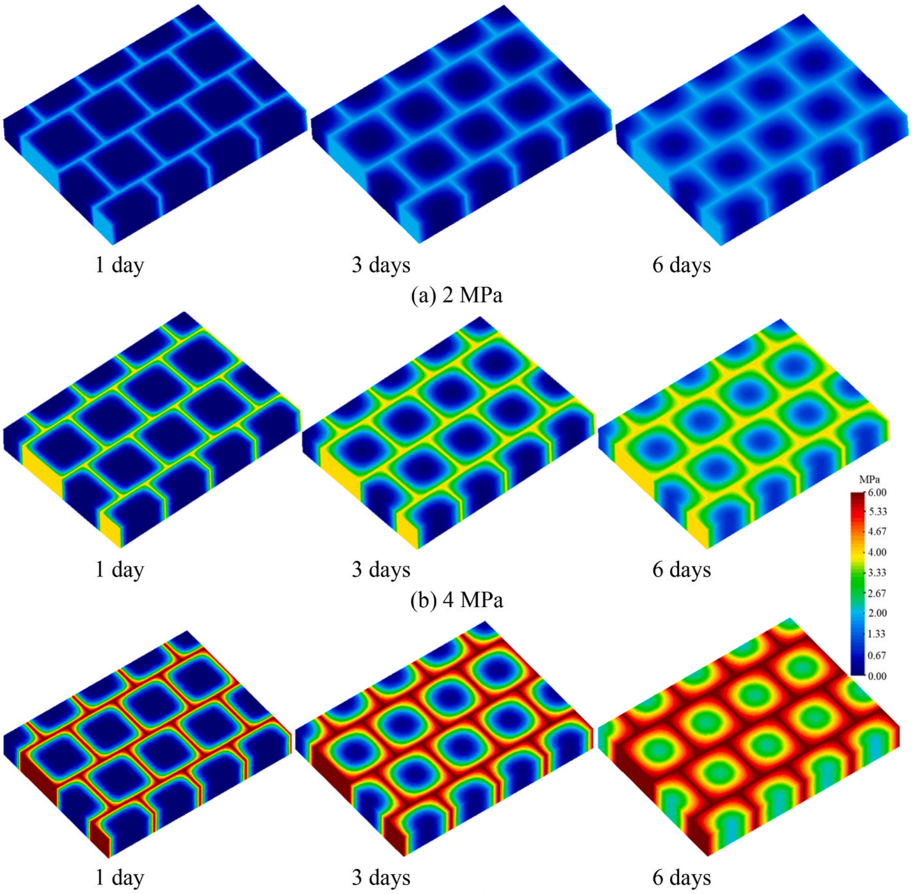

Fig. 11. Spatial distributions of gas pressure in both cleats and coal matrice.

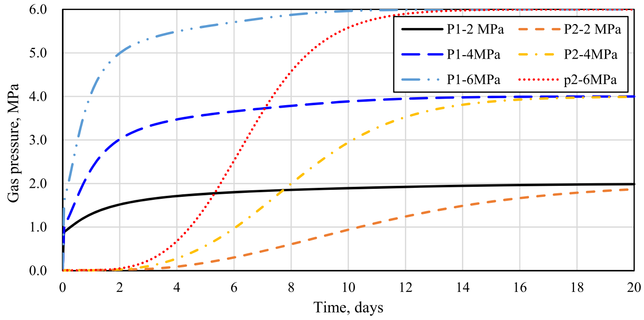

Fig. 12. Evolution of gas pressure at both detection points with gas adsorption.

and vertical displacement is assigned to bottom surface. It is assumed that the coal seam is 450 m in depth, a stress of 11.3 MPa is applied on the top surface and the horizontal stress is 7.9 MPa. It is assumed that no gas is initially present in the model domain. The parameters used for numerical simulation is listed in Table 3, and the parameters related with gas adsorption behavior and mechanical deformation are selected from literature (Chen et al., 2020a, 2020b; Cui et al., 2007).

5.2. Results and discussion

5.2.1. Evolution of pressure and adsorbed gas concentration

Fig. 11 shows the spatial distribution of gas pressure in both cleat network and coal matrix after 1 day, 3 days and 6 days. It can be seen that the gas pressure in the cleat increases to boundary pressure immediately due to higher conductivity of cleats and the gas pressure in cleats are identical. Meanwhile, gas pressure in matrix increases gradually, especially in the centre of the matrix. Fig. 11 shows that the required time to reach the equilibrium state varies with boundary pressures. When boundary pressure is 2 MPa, the gas front does not reach to the centre of matrix blocks even after 6 days. However, the gas pressure experiences an obvious increase in the centre of matrix block when boundary pressure is 4 MPa or 6 MPa. This suggests that the diffusion behavior of gas in coal matrices is pressure dependent.

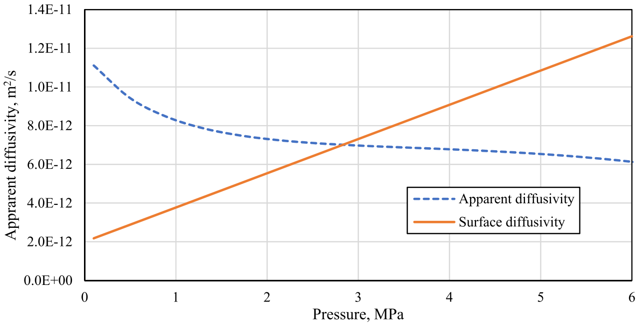

Fig. 13. Changes in diffusivities of free phase and adsorbed phase with pressure.

The variation of gas pressures at the P1 and P2 observation points for different pressure boundary values is shown in Fig. 12. As expected, the pressure evolutions are different for different boundary pressures, especially in the vicinity of cleats and centre of matrix block is

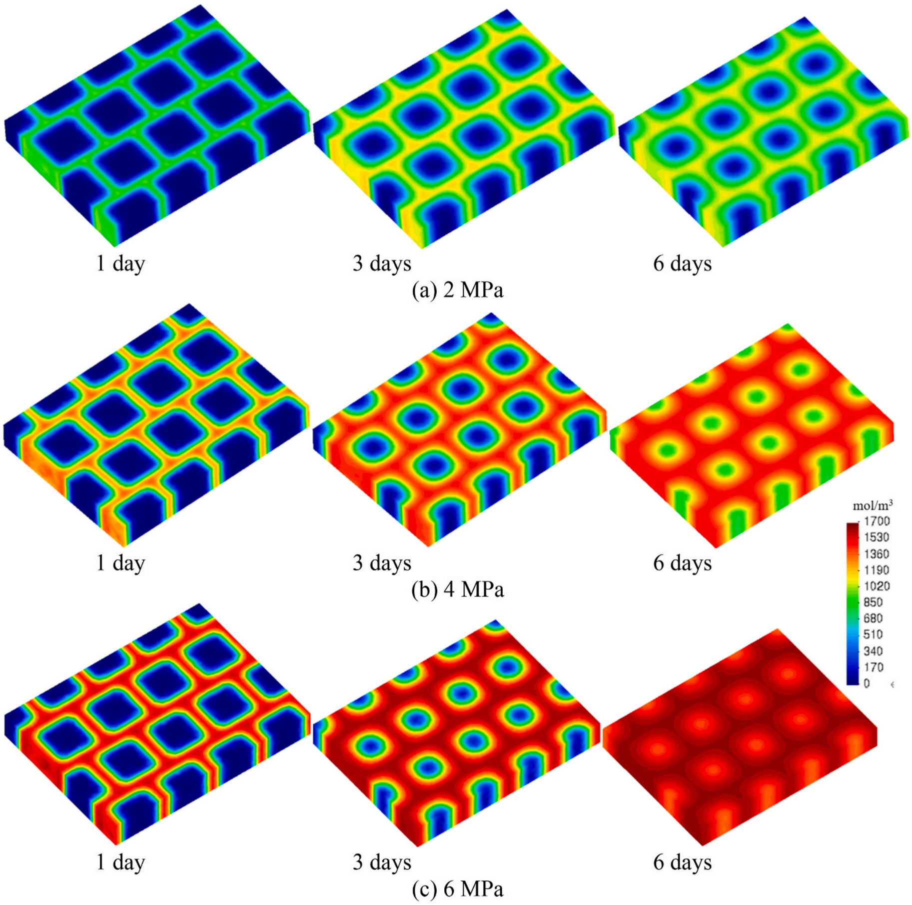

(a) 2 MPa

(b) 4 MPa

(c) 6 MPa

Fig. 14. Spatial distributions of adsorbed gas concentration in the coal matrix.

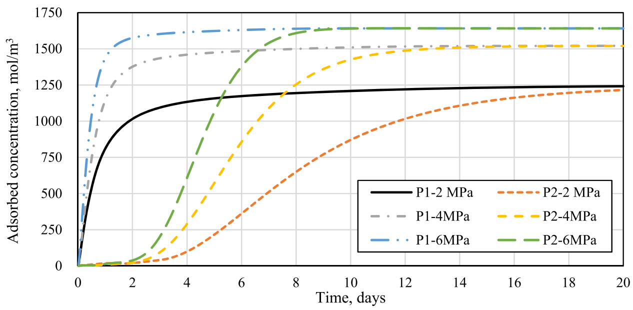

Fig. 15. Evolution of adsorbed concentration at both detection points.

significantly different. It is observed that the gas pressure at P1 (near cleats) increases rapidly at the early stages, and then gradually before reaching the equilibrium state. The lower the gas pressure at the boundary the longer it takes to reach equilibrium. For example, when the applied boundary pressure is 2 MPa, the gas pressure in coal matrices can not reach equilibrium state even after 20 days, shown in Fig. 11. However, it takes approximately 18 days and 14 days for gas pressure to reach equilibrium when the applied pressure at the boundary is 4 MPa and 6 MPa, respectively. This can be due to either i) higher pressure which can form larger pressure gradient and ii) higher pressure that causes a significant increase in surface diffusion as a result of more gas adsorption in coal matrices, shown in Fig. 13. Although the apparent diffusivity (defined as $\omega_K D_K + \omega_v D_v$) drops with increase in gas pressure, as illustrated in Fig. 13, this decrease is not significant when pressure is higher. In contrast, the surface diffusion experiences an obvious rise. This implies that the surface diffusion is an important diffusion mechanism when pressure is higher.

Fig. 14 shows the spatial distribution of adsorbed gas concentration in coal matrices after 1 day, 3 days and 6 days and Fig. 15 presents the evolution of adsorbed gas concentration at both detection points, i. e, P1 and P2. As gas diffuses from cleats to coal matrices, free phase gas will adsorbs onto the pore surface of coal matrices, and adsorbed gas concentration increases with time. However, the increase in adsorbed gas concentration at higher boundary pressure is slow. The increase in gas adsorption concentration resulting from gas pressure increasses from 2 MPa to 4 MPa doubles compared to that due to gas pressure increasses from 4 MPa to 6 MPa, since the gas adsorption follows Langmuir isotherm, as shown in Fig. 15.

It is worth mentioning that compared to the gas pressure distribution, adsorbed gas fronts advances inward in coal matrices ahead of gas pressure front. This is also reflected by the shorter time required for adsorbed gas reaching equilibrium compared to that for gas pressure, as shown in Fig. 15. Adsorbed gas migration relys on surface diffusion, which is a concentration dependent diffusion mechanism. The surface diffusion coefficient can increase with adsorbed gas concentration or pressure (see Fig. 13). Due to higher adsorbed gas concentration at larger pressure, the surface diffusion coefficient is larger; also when gas pressure is higher, more adsorbed gas can flow inward. If the gas pressure is not large enough, the adsorption equilibrium can not be reached, and the adsorbed gas will evaporate from pore surface of matrices and become free gas to increase gas pressure. This can explain why the time required for adsorbed gas reaching maximum value is less than that for gas pressure, especially for larger pressure boundaries.

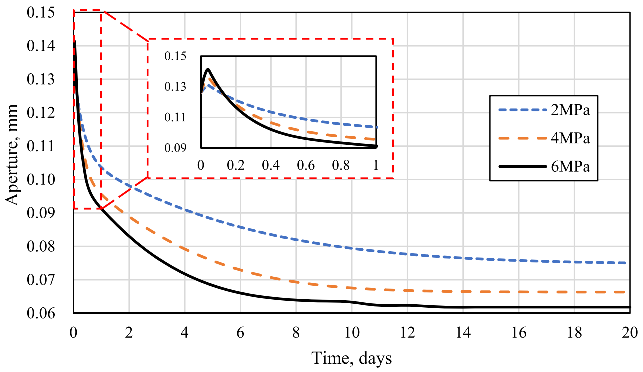

Fig. 16. Cleat aperture evolution with time.

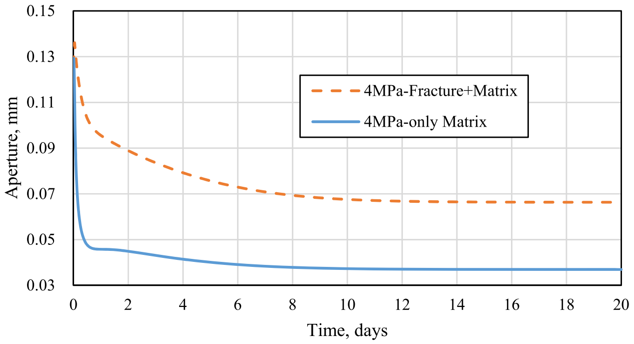

Fig. 17. Comparison of cleat aperture evolution.

5.2.2. Evolution of cleat aperture

The cleat network plays an important role in gas migration during coalbed methane recovery or carbon dioxide sequestration in unminable coal seams. Especially at field scale, it provides the most likely pathway for the transmission of fluid in coal seams. This work represents the variation of cleat aperture explicitly as a result of change in stress field. Fig. 16 shows the cleat aperture evolution under boundary pressure of 2, 4 and 6 MPa. It can be observed that the aperture initially experiences a slight opening. This is because the fluid pressure increase in cleat network leads to drop in normal stress acting on surfaces of cleats. As time increases, and free gas diffuses into coal matrices and adsorbers onto the pore surface, this causes coal swelling deformation. Because of constraint on horizontal displacement, the compression stress on the cleat surface increases and causes the closure of cleat. Fig. 16 shows that there is a rapid decrease in cleat aperture at early stage due to less normal stiffness, which is however reduced gradually with time. This is because the normal stiffness increases with the closure of cleat, and larger stress is required to compress the cleat. Higher gas pressure enables faster diffusion of gas into coal matrices, leading to a faster drop in aperture at early stages compared to those caused by lower pressure.

Fig. 17 compares the aperture calculated with and without considering fracture deformation. The later can be achieved by defining a larger cleat spacing. The injection gas pressure is 4 MPa. Without considering nonlinear fracture deformation, the change in aperture is overestimated considerably. The aperture is 0.037 mm after reaching equilibrium state, while it doubles when considering fracture stiffness. Importantly, the predicted aperture experiences much faster drop when only coal matrix deformation is considered. This implies that the aperture deformation mainly depends on the swelling of coal matrices in the vicinity of cleats. However, when considering fracture deformation, the aperture evolution takes longer to reach equilibrium state. This suggests that when evaluating the permeability of fractured media, the effect of fracture stiffness on deformation should be taken into account.

6. Conclusions

Fluid flow in deformable fractured coals is a complex process due to its unique structure. To understand the coupling of compressible flow, adsorption and deformation in a fractured coal, a discrete fracture matrix modelling approach is adopted to model the coupled hydro-mechanical behavior occurring at the cleat scale of a coal reservoirs. The flow in fractures is represented explicitly with lower-dimensional interface elements. The model considers the free gas phase and the adsorbed gas phase individually based on different gas transport mechanisms. Both phases interlink via mass exchange between the phases, which is represented via the Langmuir kinetics. The equivalent poroelastic continuum model is applied to lump the deformation of both coal matrix and fracture together. The validation exercises demonstrated good agreements between the model predicted results and experimental results collected from literatures.

The numerical results indicate that the fracture network is immediately saturated with gas due to its high conductivity, and then the gas diffuses into coal matrix blocks. The diffusion of gas in coal matrices is affected by gas pressure. The required time for adsorbed gas to reach equilibrium is shorter than that of gas pressures. This suggests that the surface diffusion is dominant for gas transport in a coal matrix. Fracture opening only occurs temporarily, followed by a significant closure as a result of adsorption induced-swelling of coal matrices. Ignoring the effect of fracture on bulk deformation will overestimate the aperture change, this implies that the nonlinear fracture deformation should be considered when evaluating the permeability of fractured rock.

Credit author statement

Min Chen: Conceptualization, Data curation, Formal analysis, Writing-Original draft preparation, Methodology, Validation, Investigation, Software; **Shakil Masum:** Writing - review & editing, Project administration; **Hywel Thomas**: Funding acquisition, Supervision.

Declaration of competing interest

The authors declare the following financial interests/personal relationships which may be considered as potential competing interests: Min Chen reports financial support was provided by Research Fund for Coal and Steel.

Data availability

Data will be made available on request.

Acknowledgement

The research was conducted as part of the “Establishing a Research Observatory to Unlock European Coal Seams for Carbon Dioxide Storage (ROCCS)” project. The ROCCS project has received funding from the Research Fund for Coal and Steel under Grant Agreement No. 899336. The financial support is gratefully acknowledged.

References

Bandis, S., Lumsden, A., Barton, N., 1983. Fundamentals of rock joint deformation. Int. J. Rock Mech. Min. Sci. Geomech. Abstracts 249–268. Elsevier.
Barton, N., Bandis, S., Bakhtar, K., 1985. Strength, deformation and conductivity coupling of rock joints. Int. J. Rock Mech. Min. Sci. Geomech. Abstracts 121–140. Elsevier.
Bastola, S., Chugh, Y., 2015. Shear Strength and Stiffness of Bedding Planes and Discontinuities in the Immediate Roof Rocks Overlying the No 6 Coal Seam in Illinois, 13th ISRM International Congress of Rock Mechanics. International Society for Rock Mechanics and Rock Engineering.

Bertrand, F., Buzzi, O., Collin, F., 2019. Cleat-scale modelling of the coal permeability evolution due to sorption-induced strain. Int. J. Coal Geol. 216, 103320.

Bertrand, F., Cerfontaine, B., Collin, F., 2017. A fully coupled hydro-mechanical model for the modeling of coalbed methane recovery. J. Nat. Gas Sci. Eng. 46, 307–325.

Busch, A., Gensterblum, Y., Krooss, B.M., Littke, R., 2004. Methane and carbon dioxide adsorption–diffusion experiments on coal: upscaling and modeling. Int. J. Coal Geol. 60, 151–168.

Charrière, D., Pokryszka, Z., Behra, P., 2010. Effect of pressure and temperature on diffusion of CO_2 and CH_4 into coal from the Lorraine basin (France). Int. J. Coal Geol. 81, 373–380.

Chen, M., Hosking, L.J., Sandford, R.J., Thomas, H.R., 2020a. A coupled compressible flow and geomechanics model for dynamic fracture aperture during carbon sequestration in coal. Int. J. Numer. Anal. Methods Geomech. 44 (13), 1727–1749.

Chen, M., Masum, S., Thomas, H., 2020b. Modeling non-isothermal transport behavior of real gas in deformable coal matrix. Energy Fuel. 35, 1605–1619.

Chen, M., Masum, S., Thomas, H., 2021. Modeling adsorption and transport behavior of gases in moist coal matrix. Energy Fuel. 35, 13200–13214.

Chen, M., Masum, S.A., Thomas, H.R., 2022. 3D hybrid coupled dual continuum and discrete fracture model for simulation of CO_2 injection into stimulated coal reservoirs with parallel implementation. Int. J. Coal Geol. 262, 104103.

Chen, Y., Yang, R., 1991. Concentration dependence of surface diffusion and zeolitic diffusion. AIChE J. 37, 1579–1582.

Cho, S., Kim, S., Kim, J., 2019. Life-cycle energy, cost, and CO_2 emission of CO_2-enhanced coalbed methane (ECBM) recovery framework. J. Nat. Gas Sci. Eng. 70, 102953.

Civan, F., 2010. Effective correlation of apparent gas permeability in tight porous media. Transport Porous Media 82, 375–384.

Clarkson, C., Bustin, R., 1999. The effect of pore structure and gas pressure upon the transport properties of coal: a laboratory and modeling study. 2. Adsorption rate modeling. Fuel 78, 1345–1362.

Cui, L.-Y., Masum, S.A., Ye, W.-M., Thomas, H.R., 2022. Investigation on gas migration behaviours in saturated compacted bentonite under rigid boundary conditions. Acta Geotech. 17, 2517–2531.

Cui, X., Bustin, R.M., Chikatamarla, L., 2007. Adsorption-induced coal swelling and stress: implications for methane production and acid gas sequestration into coal seams. J. Geophys. Res. 112.

Cui, X., Bustin, R.M., Dipple, G., 2004. Selective transport of CO_2, CH_4, and N_2 in coals: insights from modeling of experimental gas adsorption data. Fuel 83, 293–303.

Czaplinski, A., Gustkiewicz, J., 1990. Sorption stresses and deformations in coal. Strata Multiph. Med. 455–468 (in Polish, Eng ver prov by second auth) 2.

Darabi, H., Ettehad, A., Javadpour, F., Sepehrnoori, K., 2012. Gas flow in ultra-tight shale strata. J. Fluid Mech. 710, 641–658.

Do, D., Wang, K., 1998. A new model for the description of adsorption kinetics in heterogeneous activated carbon. Carbon 36, 1539–1554.

Gu, F., Chalaturnyk, R., 2006. Numerical simulation of stress and strain due to gas sorption/desorption and their effects on in situ permeability of coalbeds. J. Can. Petrol. Technol. 45.

Gu, F., Chalaturnyk, R., 2010. Permeability and porosity models considering anisotropy and discontinuity of coalbeds and application in coupled simulation. J. Petrol. Sci. Eng. 74, 113–131.

Hosking, L.J., Chen, M., Thomas, H.R., 2020. Numerical analysis of dual porosity coupled thermo-hydro-mechanical behaviour during CO_2 sequestration in coal. Int. J. Rock Mech. Min. Sci. 135, 104473.

Javadpour, F., Fisher, D., Unsworth, M., 2007. Nanoscale gas flow in shale gas sediments. J. Can. Petrol. Technol. 46.

Laubach, S., Marrett, R., Olson, J., Scott, A., 1998. Characteristics and origins of coal cleat: a review. Int. J. Coal Geol. 35, 175–207.

Liu, H.-H., Rutqvist, J., 2010. A new coal-permeability model: internal swelling stress and fracture–matrix interaction. Transport Porous Media 82, 157–171.

Masum, S.A., Chen, M., Hosking, L.J., Stańczyk, K., Kapusta, K., Thomas, H.R., 2022. A numerical modelling study to support design of an in-situ CO2 injection test facility using horizontal injection well in a shallow-depth coal seam. Int. J. Greenh. Gas Control 119, 103725.

Omotilewa, O.J., Panja, P., Vega-Ortiz, C., McLennan, J., 2021. Evaluation of enhanced coalbed methane recovery and carbon dioxide sequestration potential in high volatile bituminous coal. J. Nat. Gas Sci. Eng. 91, 103979.

Pan, Z., Connell, L.D., 2012. Modelling permeability for coal reservoirs: a review of analytical models and testing data. Int. J. Coal Geol. 92, 1–44.

Peng, D.-Y., Robinson, D.B., 1976. A new two-constant equation of state. Ind. Eng. Chem. Fundam. 15, 59–64.

Pillalamarry, M., Harpalani, S., Liu, S., 2011. Gas diffusion behavior of coal and its impact on production from coalbed methane reservoirs. Int. J. Coal Geol. 86, 342–348.

Poling, B.E., Prausnitz, J.M., O'connell, J.P., 2001. The Properties of Gases and Liquids. Mcgraw-hill, New York.

Pone, J.D.N., Halleck, P.M., Mathews, J.P., 2009. Sorption capacity and sorption kinetic measurements of CO_2 and CH4 in confined and unconfined bituminous coal. Energy Fuel. 23, 4688–4695.

Sadasivam, S., Masum, S., Chen, M., Stanczyk, K., Thomas, H., 2022. Kinetics of gas phase CO_2 adsorption on bituminous coal from a shallow coal seam. Energy Fuel. 36, 8360–8370.

Seidle, J., 2011. Fundamentals of Coalbed Methane Reservoir Engineering. PennWell Books.

Shi, J., Durucan, S., 2003. A bidisperse pore diffusion model for methane displacement desorption in coal by CO_2 injection. Fuel 82, 1219–1229.

Thomas, H., He, Y., 1995. Analysis of coupled heat, moisture and air transfer in a deformable unsaturated soil. Geotechnique 45, 677–689.

Thomas, H., Rees, S., Sloper, N., 1998. Three-dimensional heat, moisture and air transfer in unsaturated soils. Int. J. Numer. Anal. Methods GeoMech. 22, 75–95.

van Golf-Racht, T.D., 1982. Fundamentals of Fractured Reservoir Engineering. Elsevier.

Vangkilde-Pedersen, T., Anthonsen, K.L., Smith, N., Kirk, K., van der Meer, B., Le Gallo, Y., Bossie-Codreanu, D., Wojcicki, A., Le Nindre, Y.-M., Hendriks, C., 2009. Assessing European capacity for geological storage of carbon dioxide–the EU GeoCapacity project. Energy Proc. 1, 2663–2670.

Villazon, M., German, G., Sigal, R.F., Civan, F., Devegowda, D., 2011. Parametric investigation of shale gas production considering nano-scale pore size distribution, formation factor, and non-Darcy flow mechanisms. In: SPE Annual Technical Conference and Exhibition. Society of Petroleum Engineers.

Wang, G., Ren, T., Qi, Q., Lin, J., Liu, Q., Zhang, J., 2017. Determining the diffusion coefficient of gas diffusion in coal: development of numerical solution. Fuel 196, 47–58.

Weniger, S., Weniger, P., Littke, R., 2016. Characterizing coal cleats from optical measurements for CBM evaluation. Int. J. Coal Geol. 154, 176–192.

Wu, K., Chen, Z., Li, X., Guo, C., Wei, M., 2016. A model for multiple transport mechanisms through nanopores of shale gas reservoirs with real gas effect–adsorption-mechanic coupling. Int. J. Heat Mass Tran. 93, 408–426.

Xiong, X., Devegowda, D., Villazon, M., German, G., Sigal, R.F., Civan, F., 2012. A fully-coupled free and adsorptive phase transport model for shale gas reservoirs including non-Darcy flow effects. In: SPE Annual Technical Conference and Exhibition. Society of Petroleum Engineers.

Zhao, W., Cheng, Y., Pan, Z., Wang, K., Liu, S., 2019. Gas diffusion in coal particles: a review of mathematical models and their applications. Fuel 252, 77–100.